Title: Carbon dots from tryptophan doped glucose for peroxynitrite sensing

Author: Eliana F.C. Simõ es Joaquim C.G. Esteves da Silva João M.M. Leitão

PII: S0003-2670(14)01054-X
DOI: http://dx.doi.org/doi:10.1016/j.aca.2014.08.050
Reference: ACA 233450

To appear in: *Analytica Chimica Acta*

Received date: 16-5-2014
Revised date: 28-7-2014
Accepted date: 25-8-2014

Please cite this article as: Eliana F.C.Simõ es, Joaquim C.G.Esteves da Silva, João M.M.Leitão, Carbon dots from tryptophan doped glucose for peroxynitrite sensing, Analytica Chimica Acta http://dx.doi.org/10.1016/j.aca.2014.08.050

Carbon dots from tryptophan doped glucose for peroxynitrite sensing

Eliana F. C. Simões[a,b], Joaquim C.G. Esteves da Silva[b]and João M.M. Leitão[a,*]

[a] CIQ-UP, Grupo de Ciências Biológicas e Bioanalíticas, Faculdade de Farmácia da Universidade de Coimbra, Pólo das Ciências da Saúde, 3000-548 Coimbra, Portugal

[b] CIQ-UP, Departamento de Química, Faculdade de Ciências da Universidade do Porto, R. Campo Alegre 687, 4169-007 Porto, Portugal

[*]**Corresponding author:** Tel.: +351 239 488 465; e-mail address:jleitao@ff.uc.pt

Graphical abstract

fx1

Highlights

- Synthesis of tryptophan doped carbon dots.
- Experimental design optimization ofthe tryptophan doped carbon dots synthesis.
- Fluorescence sensingof peroxynitriteby tryptophan doped carbon dots.
- Peroxynitrite quantification in serum samplesby tryptophan doped carbon dots.

Abstract

Tryptophan doped carbon dots (Trp-CD) were microwave synthesized. The optimum conditions of synthesizingof the Trp-CDwere established by response surface multivariate optimization methodologies and were the following: 2.5 g of glucose and 300 mg of tryptophan diluted in 15 mL of water exposed for 5 minutes to a microwave radiation of 700 W. Trp-CD have an average size of 20 nm, were fluorescent with a

quantum yield of 12.4% and the presence of peroxynitrite anion ($ONOO^-$) provokes quenching of the fluorescence. The evaluated analytical methodology for $ONOO^-$ detection shows a linear response range from 5 to 25 µM with a limit of detection of 1.5 µM and quantification of 4.9 µM. The capability of the $ONOO^-$ quantification was evaluated in standard solutions and in fortified serum samples.

Keywords: Carbon dots; Tryptophan; Peroxynitrite; Sensing; Fluorescence quenching

1. Introduction

Peroxynitrite anion ($ONOO^-$), one of the mainreactive oxygen and nitrogen species(ROS/RNS), is implicated in several physiological or pathological processes.The formation of $ONOO^-$*in vivo*is the result of the fast reaction between nitric oxide (NO) and superoxide ($O_2^{\cdot-}$) radicals. The $ONOO^-$is unstable in acid mediumbut relatively stable in basic solution. AtpH lower than 7.4 $ONOO^-$ is protonated,forming the peroxynitrous acid (ONOOH, pK_a = 6.8), followed by decomposition to nitrate [1-3].

The $ONOO^-$ is a strong oxidant and a powerful nitration agent of biomolecules, including proteins, resulting in the modification oftheir structures and functions. Some of the reactions of $ONOO^-$ with proteins occurthrough a direct reaction with the cysteine, methionine and tryptophanamino acids residues. Beside this reaction pathway, also the reaction of $ONOO^-$ with proteins could occur through the direct reaction with transition metal centres and selenium-containing aminoacids or indirectly by the reaction of secondary $ONOO^-$derived radicals (hydroxyl, nitrogen dioxide and carbonate radical) with protein residues[3].

Due to the biological role of $ONOO^-$, analytical methodologies for its detection or quantification are of outstanding relevance. However, its reactivity, short half-life, rapid

diffusion, low concentration, antioxidant mechanisms, participation in several oxidation and nitration reactions and the presence of possible interferences, makes the detection of $ONOO^-$ challenging [1, 2, 4-6].Most of the analytical methodologies for $ONOO^-$ arebased in is reactivity. Based on is nitrating ability, the detection of $ONOO^-$ was done through the detection of the product of the tyrosine nitration (3-nitrotyrosine) by immunochemical or chromatographic techniques [4, 7-9] andof tryptophan nitration (5- and 6-nitrotryptophan) by liquid-chromatography-mass spectrometry (LC-MS)[10].The fluorescence and chemiluminescence detection of $ONOO^-$is based on is oxidation capability. A great number of organic fluorophores probes as the fluorescein [5, 8, 11-18] and rhodamine [12, 19]derivatives were oxidized by the $ONOO^-$and the related fluorescent oxidation product was evaluated.Fluorescence quenching methods based in the oxidation by the $ONOO^-$of folic acid [20] or L-tyrosine [21] and chemiluminescence methods based in the quantitativeoxidation of the chemiluminescence probes luminol and coelenterazine [5] were developed.

Carbon dots (CD)are fluorescent nanoparticles with attractive analytical properties such water solubility,high quantum yield fluorescence, high biocompatibility and good photostability[22, 23].They can be synthesised by several methods using different carbon precursors[24]. Microwave assisted CD synthesis is a straightforward methodology and several precursors can be used, for example:carbohydrates[25, 26], PEG[27], citric acid[28] and dopamine[29].Due to their fluorescence characteristics, the CD have been proposed for the fluorescence sensing of different analytes [22, 24]. For the direct detection of $ONOO^-$ by nanoparticles a quenching fluorescent method based in thiol-capped CdTe or CdTe/ZnS quantum dots (QD)[30] and a colorimetric methodology based on Au nanoparticles have now been proposed [31].For the fluorescencethiol-capped QD

methodology a limit of detection (LOD)of 0.01,0.02 and 0.07 μM at a pH 9.4 and for the colorimetric Au nanoparticles a linear range from 9.78 to 20.77 mMwerecalculated.

In this paper we describe the design and synthesis of CD for $ONOO^-$ detection and quantification. Taking into consideration the nitration and oxidation potential of $ONOO^-$, the amino acid tryptophan was used to dope a carbohydrate (glucose) precursor, in order to make them reactive towards peroxynitrite anion. In this study,glucose(Bare-CD) and tryptophan doped glucose (Trp-CD) were used as CD precursors using a microwave pyrolysis methodology. The synthesis process of these two CD samples, Bare-CD and Tryp-CD, were optimized using multivariate experimental design methodology. The potential of the CD nanoparticles as $ONOO^-$ sensor was evaluated. Trp-CDsynthesized in the presence of glucose and tryptophan has been showed an improvement in the quantum yield(Φ) comparatively to Bare-CD prepared only from glucose and showed a greater sensibility to the $ONOO^-$ presence probably due to the oxidation of tryptophan added to CDfunctionalization.

2. Experimental

2.1. Reagents

Tryptophan, hydrogen peroxide (H_2O_2), sodium hydroxide (NaOH), hydrogen chloride (HCl), sodium phosphate dibasic, monosodium phosphate,potassium superoxide (KO_2), potassium iodide (KI)and sodium nitrite ($NaNO_2$) analytical grade reagents were purchased from Merck, Darmstadt (Germany).Glucose was purchased from Sigma–Aldrich Quimica S.A. (Spain). Mili-Q water with resistivity of 18.2 MΩ.cm at 25 ºC was used in all experiments.

2.2. Solutions

The $ONOO^-$ andNO standard solutions were prepared as in [13].The $O_2^{\cdot -}$ and H_2O_2 standard solutions were prepared by rigorous weighing of KO_2 and by rigorous measurement of the required volume of H_2O_2in deoxygenated water. Diluted standard solutions of the ROS/RNS were prepared by rigorous dilution of the initial standard solutions for $ONOO^-$ in NaOH 0.1 M and for NO, $O_2^{\cdot -}$ and H_2O_2 in deoxygenated water.

The $ONOO^-$quantification evaluations were performed controlling the pH at 7.4 (neutral physiological pH). Phosphate buffer pH 7.4 was preparedthrough rigorous weightingof sodium phosphate dibasic and monosodium phosphatefor the required volume of solution and posterior addition of NaOH or HCl 0.1 Min order to adjust the pH.In the evaluation of the pH effect in the fluorescence intensity of the synthetized Bare-CD and Trp-CD alsothe pH was adjusted with NaOH or HCl 0.1 M.

2.3. CD synthesis

Attending to the experimental designs performedin order to establish the optimum conditions of synthesis different masses of glucose and tryptophan were initially solubilizedin water and posterior heated in a domestic microwave at the maximum power of 700 W at different heating times. Subsequently the solutions were leaving to cool and were dissolved in water. The obtained solutions were then centrifuged at 9000 rpm for 10 min in order to remove the suspended impurities and a volume of 30 mL were set with water.

2.3.1Experimental design optimization

Optimization using response surface experimental design methodologies were used in order to establish the more adequate conditions to the Trp-CD synthesis [32-34].An

evaluation of the optimum conditions to the Bare-CD synthesis was previous done. Initial screening fractional or full factorial and posterior optimization central composite experimental designs were implemented with the Unscrambler® software version 7.51, Camo ASA, Norway.

The evaluation of the results found by the experimental design optimization of the Bare and Trp-CD synthesis was performed as previously described[13]. Only for the screening fractional factorial experimental design the initially evaluation of the main effects and variable interactions was done by a Comparison with a Scale-Independent Distribution (COSCIND) instead by a Higher Orders Interactions Effects (HOIE).

2.4. Instrumentation

2.4.1. Spectrophotometric measurements

The absorbance andthe fluorescence spectra were collected respectively in a Jasco V-530 UV-Visiblespectrophotometer and FP-6200 spectrofluorimeter in the required conditions. The reaction time profiles were obtained at the maximum emission wavelength of 496nm for Bare-CD and of 470nm for Trp-CD by an optical fiber spectrophotometer using a QE65000 charge-coupled detector and a 380 nm light emitting diodefrom Ocean Optics.

The fluorescence quantum yieldof the CD was evaluated comparing the integrated photoluminescence intensities and the absorbance values of the CD with the ones of the quinine sulphate reference.

$$\Phi = \Phi_R \times \frac{Grad}{Grad_R} \times \frac{\eta^2}{\eta_R^2}$$

In the equation Φ is the fluorescence quantum yield, *Grad* is the gradient from the plot of integrated fluorescence intensity vs. absorbance and η is the refractive index. The

subscript *R* refers to reference fluorophore quinine sulphate of known Φ. The literature Φ of the quinine sulphate is Φ=0.54[30].The η of the quinine sulphate in 0.1M H_2SO_4 and of CDaqueous solutions used were η = 1.33.

The fluorescence lifetimes were calculated using a Horiba Jovin Yvon Fluoromax 4 TCSPC spectrophotometer and the corresponding software (Decay Analysis Software v. 6.4.1, Horiba Jovin Yvon). Fluorescence decays were interpreted in terms of a multi-exponential function: $I(t) = A+\Sigma B_i \exp -t/\tau_i$, where A and B_i are the pre-exponential factors and τ_i the decay times.

The Fourier transform infrared (FTIR) spectra were obtained by a Perkin Elmer FTIR Spectrum 400 spectrophotometer in solid state with an attenuated total reflectance (ATR) accessory in a range of 4000 cm^{-1} to 650 cm^{-1} with 16 accumulationsand resolution of 2 cm^{-1}.

The X-ray photoelectron spectroscopy (XPS) analysis was performed using a Kratos AXIS Ultra HSA, with VISION software for data acquisition and CASAXPS software for data analysis. The analysis was carried out with a monochromatic Al Kα X-ray source (1486.7 eV), operating at 15kV (90 W), in FAT mode (Fixed Analyzer Transmission), with a pass energy of 40 eV for regions ROI and 80 eV for survey. Data acquisition was performed with a pressure lower than $1x10^{-6}$ Pa, and it was used a charge neutralization system. The effect of the electric charge was corrected by the reference of the carbon peak (285 eV). The deconvolution of spectra was carried out using CasaXPS programs, in which a peak fitting is performed using Gaussian-Lorentzian peak shape and Shirley type background subtraction.

2.4.2. Particle size measurements

For the evaluation by experimental design synthesis optimization the particle size of CD and their frequency size distribution was obtained by dynamic light scattering (DLS) in a Nano Delsa C, Beckman Coulter.The size and shape of thesynthetized CD in the optimum synthesis conditions were also posteriors evaluated by transmission electronic microscopy (TEM) analysis in a Fei Company Tecnai G2 20 S-Twin electronic microscopic.

3. Results and discussion

3.1. CD synthesis

An optimisation of CD synthesis was done by experimental designs methodologies in order to define the best conditions for the Bare-CD and Trp-CD synthesis (supplementary information).

Bare-CD were synthesized from microwave treatment of aqueous solutions of glucose. The objective is to obtain CD with the highest quantum yield and smaller size the possible under this bottom up procedure. In order to optimize these CD features an experimental design of the factors microwave time, mass of glucose and volume of water was done. Bare-CD with the highest fluorescence intensity and smaller size were obtained from 15 mL of water, 5 g of glucose and 9 minutes of microwave time.

The optimization of the synthesis of the CD from glucose doped with tryptophan (Trp-CD) followed a similar strategy to that of Bare-CD but one more factor was under analysis, the mass of tryptophan. Trp-CD with the highest fluorescence intensity and smaller size were obtained from 15 mL of water, 2.5 g of glucose, 300 mg of tryptophan and 5 minutes of microwave time.

3.2. CD characterization

The excitation-emission matrices (EEM) of Bare-CD and Trp-CD are shown in Fig. 1. The analysis of these EEM shows that they are quite different and that corresponding of Trp-CD are characterized by several bands in contrast with Bare-CD that shows only one fluorescence band. A detailed analysis of the EEMof Trp-CD shows:

(i) A band at the same excitation wavelength (370 nm)of the found with the Bare-CD witha slightly different emission wavelength (Bare-CD – 486 nm; Trp-CD – 457 nm) but with a marked differenceof the fluorescence intensity (Bare-CD - 44.6; Trp-CD - 604.4).

(ii)One band at excitation wavelength 270 nm and emission wavelength at 360 nm that could be assigned to the tryptophan residue; and,two other bands at excitation wavelengths (260 and 300 nm)with the same emission wavelength of 457 nm.

The analysis of the Φ of Trp-CD shows a marked increase of 34 times (Φ = 12.4) when compared to that obtained for the Bare-CD (Φ = 0.36). The lifetime decay curves of the fluorescence emission of both CD samples are quite different, and its comparison shows that Trp-CD have components with longer lifetime than Bare-CD. Multicomponent decay models adequately fit the data: Bare-CD - three component decay time model (χ^2=1.58) with lifetimes τ_1=2.77 ns, τ_2=0.53 ns and τ_3=6.80; Trp-CD - five component decay time model (χ^2=1.36) with lifetimes τ_1=0.94 ns, τ_2=0.89 ns, τ_3=0.03 ns, τ_4=21.54 ns and τ_5=5.67 ns (supplementary information). This analysis confirms that the fluorescence lifetime of Trp-CD is longer and is a mixture of fluorophores more complex than that observed for Bare-CD, and shows that tryptophan doping of glucose increases the lifetime

as well as the quantum yield.These results confirms that the tryptophan doping have a strong effect on the luminescence properties of the CD.

The mechanism that could explain the fluorescence properties of CD is related to the existence of surface defects and presence of oxygen functional groups [22]. In order to assess if the fluorophores present in Trp-CD are located in the surface of the nanoparticles, iodide anion was added and the dynamic quenching of the fluorescence was measure. The linearization of the quenching profiles observed at the maximum of the four emission bands of Trp-CD with a modified Stern-Volmer equation show that all the fluorophores are localized at the surface of the nanoparticle but the fluorophores responsible for the band with excitation 270 nm and emission 360 nm. Indeed, only 73% of this class of fluorophores is localized at the surface of the nanoparticles at accessible positions to iodide(supplementary information). This characteristic is justified because these fluorophores correspond to tryptophan residues and are distributed for all over the nanomaterial.

The effect of the pH, temperature and ionic strength in the maximum fluorescence intensity of the bands of Bare-CD and Trp-CD was studied (supplementary information). The pH has a marked effect in the fluorescence intensity of both samples and is characterized by a general decreasing trend as the pH is raised. Increasing the temperature also provokes a decreasing trend in the fluorescence but the magnitude of the effect is smaller than that observed for the pH. The ionic strength has a relatively small effect on the fluorescence intensity of both CD with no clear trend. The stability of the fluorescence intensity of both samples of CD upon excitation was checked and, besides an initially slight decrease, the fluorescence intensity remains almost constant.

Fig. 2 shows the FTIR spectra of both CD samples. The main common bandsobserved in both CD samples are: strong band at 3300 cm^{-1}(-OH), strong band at 1020 cm^{-1} (-CO), and two weak bands at 2926 cm^{-1}(-CH) and 1650 cm^{-1}(C=C).Some clear differences aredetectedin the spectra of the two CD that are due to the -NH and -CN groupspresented in Trp-CD. The band assigned to -OH in both samples are markedly sifted (Bare-CD 3306 cm^{-1}; Trp-CD 3298 cm^{-1}),as well as the band assigned to –CO (Bare-CD 1011 cm^{-1}; Trp-CD 1024 cm^{-1}). Also two bands at 1714 cm^{-1} and 1751 cm^{-1} related to =C=O are now clearly evident in the Trp-CD spectrum.

The XPS survey spectrum of the Bare and Trp-CD and the C1s, N1s and O1s core level spectrum are presented in supplementary information. The XPS survey spectrum of the Bare and Trp-CD shows the presence of carbon (63.8% and 61.8% atomic concentration, respectively) and oxygen (34.5% and 38.2% atomic concentration, respectively) in both samples and a smaller amount of nitrogen in the Trp-CD (1.7% atomic concentration) – a residual band, probably due to nitrogen, is hardly observed in the Bare-CD survey spectrum (< 0.05%). The C1s core level spectrum of Trp-CD can be decomposed into four bands at 285.0 eV (26.7%), 286.5 eV (59.1%), 288.0 eV (12.3%) and 289.4 eV (1.9%). The main contribution at low binding energy (285.0 eV) is assigned to the presence of surface methylene group, graphitic and adventitious carbon. The band at 286.5 eV has the highest relative intensity and it may be assigned to C-OH groups. The two low intensity bands can be assigned to C=O, -COO- and C-N moieties. The C1s core level spectrum of Bare-CD has a similar shape to that of Trp-CD but with slightly different proportions: 285.0 eV (14.6%), 286.6 eV (66.1%), 287.9 eV (17.3%) and 289.3 eV (2.0%). The N 1s core level spectrum of Trp-CD can be decomposed into two contributions at 400.2 eV (78.6%) and 402.1 eV (21.4%). The main band is due to N-C structures while the

minor band is due to N=C and N-O structures. A detailed examination of the N1s core level spectrum region of Bare-CD confirms that the possible band is almost confused with the noise level. The O1s core level spectrum of Trp-CD can be decomposed into three contributions at 531.3 eV (3.7%), 532.9 eV (89.9%) and 534.1 eV (6.5%). The main contribution to the O1s core level spectrum is attributed to oxygen from alcoholic and carbonyl groups. The other minor contributions may be due to CO and/or NO surface structures. The O 1s core level spectrum of Bare-CD has a similar shape to that of Trp-CD but with slightly different proportions: 531.1 eV (1.0%), 532.9 eV (92.2%) and 534.0 eV (6.8%). These results show that the surface of both CD are oxidized with a high degree of oxygen functional structures and the Trp-CD samples also show at the surface some traces of nitrogen containing structures.

The size and shape of both CD samples were determined by TEM analysis (Fig.3). For the Bare-CD a size of 2 and up to 8 nm is observed with an elliptic or irregular shape. For Trp-CD, nanoparticles with a higher size than Bare-CD of 12 up to 29 nm,with a spherical or irregular shape are observed. A statistical evaluation of the size distribution considering a sample of 100 nanoparticles shows: Bare-CD: $\bar{x}$ = 4nm (σ = 1); Trp-CD: $\bar{x}$ = 20 nm (σ = 4).

The size distribution of both CD samples in solution was determined by DLS (supplementary information). These results confirm that Bare-CD (*D50%* = 8 nm) have a smaller particle size distribution than Trp-CD (*D50%* = 153 nm). Also, these results show an agglomeration tendency for both samples in solution which is particularly evident for Trp-CD, probably because this sample has a higher density of functional groups due to the tryptophan doping. The low evaluated potential zeta for both kinds of CD (Bare-CD, -6mV; Trp-CD, + 10 mV) confirms the agglomeration tendency of both CD. Even so,

evaluations of fluorescence intensity and the quantum yield with the time shows that the fluorescence proprieties of both CD are not affected by this agglomeration tendency.

3.3. Trp-CD $ONOO^-$ sensing

Fig. 4 presents the plots of the Bare and Trp-CD fluorescence intensity as function of the concentration of the main ROS/RNS, H_2O_2, O_2^-, NO and $ONOO^-$. The analysis of these plots shows that, although a decrease of the fluorescence of the Bare-CD is observed when increasing the ROS/RNS species concentrations, it is not analytically significant (a few fluorescence units) when compared with the quenching of fluorescence provoked by $ONOO^-$ on the fluorescence intensity of Trp-CD (more than one hundred fluorescence units).

Fig.5show typical reaction time profiles of Trp-CD with $ONOO^-$. In the range 0.5 - 25 μM alinear fit y = -6.76x -3.39 (m = 7), R = -0.9937, s_{blank} = 3.35, LOD = 1.5μM, LOQ = 5.0μM are obtained. A worse linear fit is found with a concentration range of $ONOO^-$ up to 50 μM(supplementary information). The deviation of linearity that is observed for higher $ONOO^-$ concentrations is due to the pH variations induced by the $ONOO^-$ alkaline standard concentrated solution.Comparing to the previous obtained by the already developed nanosensors [30, 31], and attending to the lowest $ONOO^-$concentration evaluated, an intermediary $ONOO^-$quantification capability by the developed nanosensor was obtained.

The quenching of the fluorescence of Trp-CD by $ONOO^-$ was studied by Stern-Volmer plots and at two temperatures (Fig. 6).The analysis of these plots show their linear trend with Stern-Volmer constants (K_{SV}) of 9900±800 (20 ºC) and 4460±190 (37 ºC) M^{-1}. Taking into consideration themagnitude of these constants and its temperature

dependencea static quenching is observed probably due to a chemical reaction between $ONOO^-$ and the tryptophan residues in the CD (nitration or oxidation reaction).

In order to assess the Trp-CD based methodology, the analysis of $ONOO^-$ was done in standard solutions and fortified serum samples. Table 1 presents the results found in this analysis which shows that good quantification results were observed with the solutions under investigation.

4. Conclusions

Relatively high quantum yield carbon nanoparticles (carbon dots-CD) were successively prepared from glucose doped tryptophan (Trp-CD) by a bottom up one step microwave synthesis. Doping with tryptophan resulted in CD with increased sensitivity and selectivy towards peroxynitrite anion. The synthesis of Trp-CD was optimized with experimental design methodologies. The synthesized carbon nanoparticles had an average size of 20.3 nm with an irregular spherical shape. The $ONOO^-$ anion provokes quenching of the fluorescence intensity of the Trp-CD probably due to the oxidation of tryptophan residues in the surface of the CD. The $ONOO^-$ detection shows a linear range from 2.5 to 25 µM with a limit of detection of 1.5 µM. The $ONOO^-$ quantification capability of the Trp-CD evaluated in standard solutions and in serum fortified samples shows adequate recoveries.

Acknowledgments A PhD grant SFRH/BD/81074/2011 to Eliana Simões from Fundação para a Ciência e Tecnologia (FCT, Lisbon) is acknowledged. The TEM analyses fromNanomaterials andMicromanufacturing group of Centre for Mechanical Engineering of the University of Coimbra (CEMUC), the XPS analysis fromthe Materials Centre of the

University of Porto (CEMUP) andthe FTIR usefrom UCQFarma, Pharmacy Faculty of the University of Coimbra are acknowledged.

References

[1] M. Valko, D. Leibfritz, J. Moncol, M.T. Cronin, M. Mazur, J. Telser, Free radicals and antioxidants in normal physiological functions and human disease, The international journal of biochemistry & cell biology, 39 (2007) 44-84.

[2] S.F. Peteu, R. Boukherroub, S. Szunerits, Nitro-oxidative species in vivo biosensing: Challenges and advances with focus on peroxynitrite quantification, Biosens. Bioelectron., 58 (2014) 359-373.

[3] B. Alvarez, R. Radi, Peroxynitrite reactivity with amino acids and proteins, Amino Acids, 25 (2003) 295-311.

[4] C. Ducrocq, B. Blanchard, B. Pignatelli, H. Ohshima, Peroxynitrite: an endogenous oxidizing and nitrating agent, Cellular and molecular life sciences : CMLS, 55 (1999) 1068-1077.

[5] G. Ferrer-Sueta, R. Radi, Chemical Biology of Peroxynitrite: Kinetics, Diffusion, and Radicals, ACS Chemical Biology, 4 (2009) 161-177.

[6] R. Radi, G. Peluffo, M.N. Alvarez, M. Naviliat, A. Cayota, Unraveling peroxynitrite formation in biological systems, Free Radical Biology and Medicine, 30 (2001) 463-488.

[7] M.M. Tarpey, D.A. Wink, M.B. Grisham, Methods for detection of reactive metabolites of oxygen and nitrogen: in vitro and in vivo considerations, American Journal

of Physiology - Regulatory, Integrative and Comparative Physiology, 286 (2004) R431-R444.

[8] M.M. Tarpey, I. Fridovich, Methods of detection of vascular reactive species: nitric oxide, superoxide, hydrogen peroxide, and peroxynitrite, Circulation research, 89 (2001) 224-236.

[9] M.R. Radabaugh, O.V. Nemirovskiy, T.P. Misko, P. Aggarwal, W.R. Mathews, Immunoaffinity liquid chromatography–tandem mass spectrometry detection of nitrotyrosine in biological fluids: Development of a clinically translatable biomarker, Analytical Biochemistry, 380 (2008) 68-76.

[10] B. Alvarez, H. Rubbo, M. Kirk, S. Barnes, B.A. Freeman, R. Radi, Peroxynitrite-Dependent Tryptophan Nitration, Chemical Research in Toxicology, 9 (1996) 390-396.

[11] A. Gomes, E. Fernandes, J.F.C. Lima, Use of Fluorescence Probes for Detection of Reactive Nitrogen Species: A Review, J Fluoresc, 16 (2006) 119-139.

[12] J.P. Crow, Dichlorodihydrofluorescein and Dihydrorhodamine 123 Are Sensitive Indicators of Peroxynitrite in Vitro: Implications for Intracellular Measurement of Reactive Nitrogen and Oxygen Species, Nitric Oxide: Biology and Chemistry, 1 (1997) 145.

[13] E.C. Simões, J.M. Leitão, J.G. Esteves da Silva, Reduced Fluoresceinamine for Peroxynitrite Quantification in the Presence of Nitric Oxide, J Fluoresc, 22 (2012) 1127-1140.

[14] A. Keller, A. Mohamed, S. Dröse, U. Brandt, I. Fleming, R.P. Brandes, Analysis of dichlorodihydrofluorescein and dihydrocalcein as probes for the detection of intracellular reactive oxygen species, Free radical research, 38 (2004) 1257-1267.

[15] R. Nakahara, T. Fujimoto, M. Doi, K. Morita, T. Yamaguchi, Y. Fujita, Fluorophotometric Determination of Hydrogen Peroxide and Other Reactive Oxygen

Species with Fluorescein Hydrazide (FH) and Its Crystal Structure, Chemical and Pharmaceutical Bulletin, 56 (2008) 977-981.

[16] K. Setsukinai, Y. Urano, K. Kakinuma, H.J. Majima, T. Nagano, Development of novel fluorescence probes that can reliably detect reactive oxygen species and distinguish specific species, The Journal of biological chemistry, 278 (2003) 3170-3175.

[17] S.L. Hempel, Y.Q. O'Malley, D.A. Wessels, D.M. Flaherty, Dihydrofluorescein diacetate is superior for detecting intracellular oxidants: comparison with 2',7'-dichlorodihydrofluorescein diacetate, 5(and 6)-carboxy-2',7'-dichlorodihydrofluorescein diacetate, and dihydrorhodamine 123, Free Radical Biology & Medicine, 27 (1999) 146-159.

[18] D. Yang, H.L. Wang, Z.N. Sun, N.W. Chung, J.G. Shen, A Highly Selective Fluorescent Probe for the Detection and Imaging of Peroxynitrite in Living Cells, Journal of the American Chemical Society, 128 (2006) 6004-6005.

[19] X.F. Yang, X.Q. Guo, Y.B. Zhao, Development of a novel rhodamine-type fluorescent probe to determine peroxynitrite, Talanta, 57 (2002) 883-890.

[20] J.C. Huang, D.J. Li, J.C. Diao, J. Hou, J.L. Yuan, G.L. Zou, A novel fluorescent method for determination of peroxynitrite using folic acid as a probe, Talanta, 72 (2007) 1283-1287.

[21] J. Liang, Z.H. Liu, R.X. Cai, A novel method for determination of peroxynitrite based on hemoglobin catalyzed reaction, Analytica Chimica Acta, 530 (2005) 317-324.

[22] J.C.G. Esteves da Silva, H.M.R. Gonçalves, Analytical and bioanalytical applications of carbon dots, TrAC Trends in Analytical Chemistry, 30 (2011) 1327-1336.

[23] Y. Zhang, H. Goncalves, J.C.G. Esteves da Silva, C.D. Geddes, Metal-enhanced photoluminescence from carbon nanodots, Chemical Communications, 47 (2011) 5313-5315.

[24] E.F. Simoes, J.M. Leitao, J.C.G. Esteves da Silva, Reduced fluoresceinamine for peroxynitrite quantification in the presence of nitric oxide, J Fluoresc, 22 (2012) 1127-1140.

[25] X. He, H. Li, Y. Liu, H. Huang, Z. Kang, S.T. Lee, Water soluble carbon nanoparticles: Hydrothermal synthesis and excellent photoluminescence properties, Colloids and Surfaces B: Biointerfaces, 87 (2011) 326-332.

[26] H. Yan, M. Tan, D. Zhang, F. Cheng, H. Wu, M. Fan, X. Ma, J. Wang, Development of multicolor carbon nanoparticles for cell imaging, Talanta, 108 (2013) 59-65.

[27] H. Zhu, X. Wang, Y. Li, Z. Wang, F. Yang, X. Yang, Microwave synthesis of fluorescent carbon nanoparticles with electrochemiluminescence properties, Chemical Communications, (2009) 5118-5120.

[28] S. Zhu, Q. Meng, L. Wang, J. Zhang, Y. Song, H. Jin, K. Zhang, H. Sun, H. Wang, B. Yang, Highly Photoluminescent Carbon Dots for Multicolor Patterning, Sensors, and Bioimaging, Angewandte Chemie International Edition, 52 (2013) 3953-3957.

[29] K. Qu, J. Wang, J. Ren, X. Qu, Carbon dots prepared by hydrothermal treatment of dopamine as an effective fluorescent sensing platform for the label-free detection of iron(III) ions and dopamine, Chemistry (Weinheim an der Bergstrasse, Germany), 19 (2013) 7243-7249.

[30] O. Adegoke, T. Nyokong, Probing the sensitive and selective luminescent detection of peroxynitrite using thiol-capped CdTe and CdTe@ZnS quantum dots, Journal of Luminescence, 134 (2013) 448-455.

[31] L. Chen, N. Wu, B. Sun, H. Su, S. Ai, Colorimetric detection of peroxynitrite-induced DNA damage using gold nanoparticles, and on the scavenging effects of antioxidants, Microchim Acta, 180 (2013) 573-580.

[32] M.A. Bezerra, R.E. Santelli, E.P. Oliveira, L.S. Villar, L.A. Escaleira, Response surface methodology (RSM) as a tool for optimization in analytical chemistry, Talanta, 76 (2008) 965-977.

[33] T. Lundstedt, E. Seifert, L. Abramo, B. Thelin, Å. Nyström, J. Pettersen, R. Bergman, Experimental design and optimization, Chemometrics and Intelligent Laboratory Systems, 42 (1998) 3-40.

[34] J.M. Leitao, J.C. Esteves da Silva, Factorial analysis optimization of a Diltiazem kinetic spectrophotometric quantification method, Analytica chimica acta, 609 (2008) 1-12.

Fig. 1 - EEM of Bare (a) and Trp-CD (b) at the optimum synthesis conditions.

Fig. 2 - FTIR spectra of Bare and Trp-CD.

Fig. 3 – Images obtained by TEM analysis of the Bare (a) and Trp-CD (b).

Fig. 4 - Effect of $ONOO^-$ on the other ROS/RNS in Bare (a) and Trp-CD (b).

Fig. 5 – Typical fluorescence time profiles of the Trp-CD by $ONOO^-$ addition.

Fig. 6 – Stern-Volmer plots at two different temperatures.

s_{xi} - interpolated standard deviation;$IC_{95\%}$ - interpolated 95 % confidence interval; *a* - intercept; s_a - intercept standard deviation; *b* - slope; s_b - slope standard deviation; $s_{y/x}$ - standard deviation of residuals; *R* - linear correlation coefficient; *m* - number of calibration points.

Fig. 1

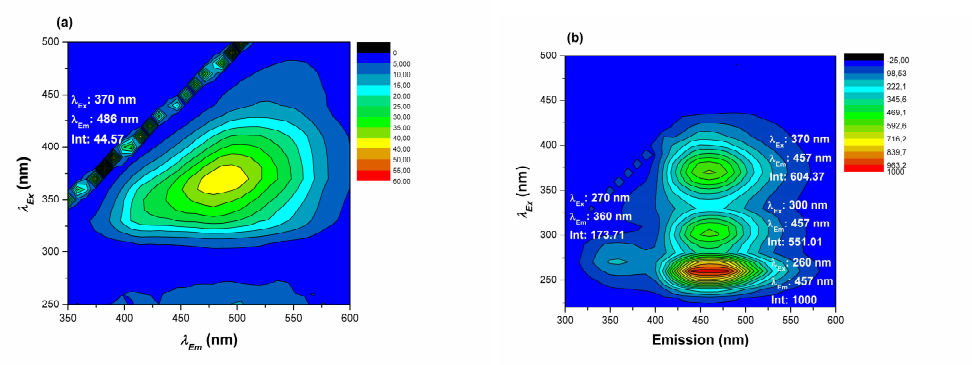

Fig. 2

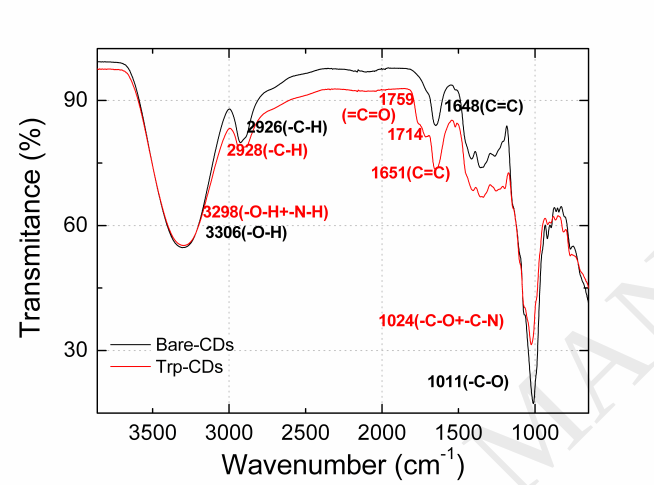

Fig. 3

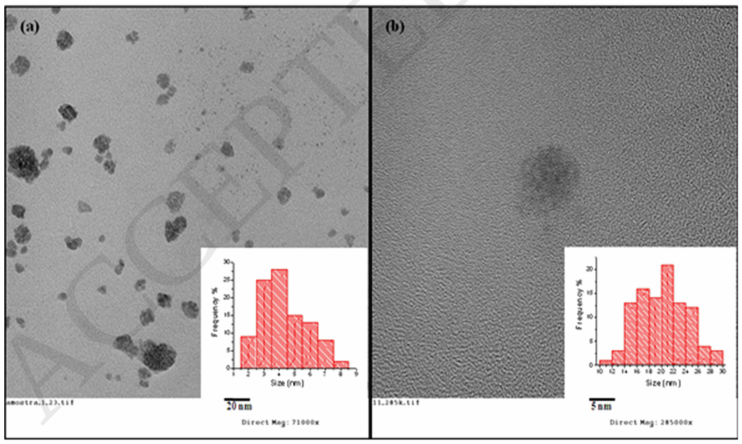

Fig. 4

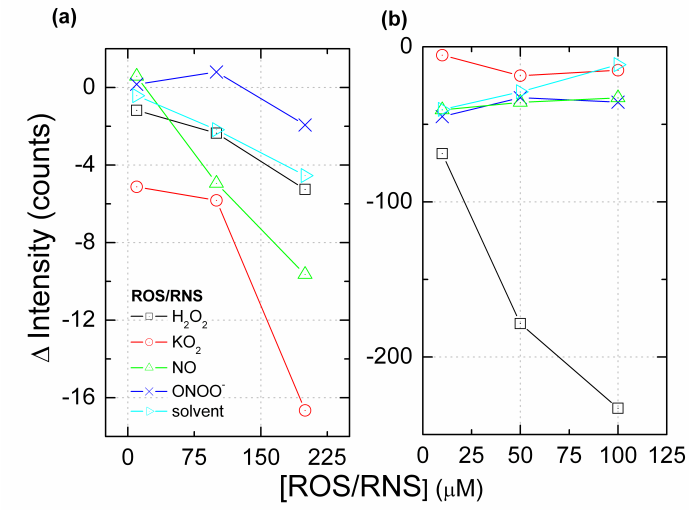

Fig. 5

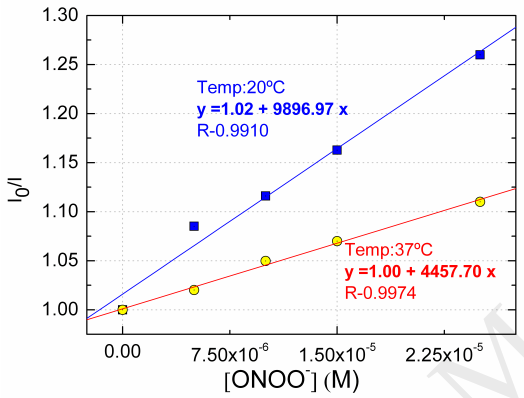

Table 1 - $ONOO^-$ quantification results in standard solutions and in fortified serum samples.

Trp-CD (m_{Glc} - 2.5 g; m_{Trp} – 300 mg; t_{mic} – 5 min)				
[$ONOO^-$] (μM)	**Standard solutions**			**Fortified serum (10 ×)**
Expected	**5**	**10**	**15**	**15**
Estimated	5.13 s_{xi}= -1.04 $IC_{95\%}$ = ± 4.48	8.78 s_{xi}= -0.97 $IC_{95\%}$ = ± 4.15	17.98 s_{xi} = -0.96 $IC_{95\%}$ = ± 4.11	15.82 s_{xi} = -2.16 $IC_{95\%}$ = ± 9.29

Recovery (%)	102.65	87.85	119.89	105.43

y = bx + a [ΔI = f([$ONOO^-$])]

a = -7.09 ; s_a= 2.83
b = -3.25; s_b= 0.18
$s_{y/x}$= 2.86 ; **R** = 0.9969
m = 4; 5 - 25 µM